International Journal of Thermal Sciences 48 (2009) 1728–1740

Contents lists available at ScienceDirect

International Journal of Thermal Sciences

journal homepage: www.elsevier.com/locate/ijts

Film boiling heat transfer around a very high temperature thin wire immersed into water at pressure from 1 to 210 bar: Experimental results and analysis

Georges Berthoud*, Luc Gros D'Aillon

CEA Grenoble, 17 rue des Martyrs, 38054 Grenoble, Cedex 9, France

ARTICLE INFO

Article history:
Received 7 October 2008
Received in revised form
20 January 2009
Accepted 23 January 2009
Available online 25 March 2009

Keywords:
Forced convection film boiling
Cross flow around cylinder
High temperature

ABSTRACT

When a hot liquid comes in contact with a more volatile one, we may observe a vapor explosion. This is due to the intense vapor production caused by the high heat transfer between micronic fragments (resulting from the fine fragmentation of the hot liquid) and the coolant. An experimental apparatus called TREPAM investigates this heat transfer. In this experiment, the coolant level rises at a constant velocity over a fixed high temperature tungsten wire. Measurement of wire electric resistivity, which is related to the wire temperature, enables the calculation of the heat transfer. This heat transfer is studied in the ranges of:

- wire diameter from 10 to 250 μm
- wire temperature from 1350 to 2900 K
- water subcooling from 0 to 350 K
- water velocity from 0.2 to 46 m/s
- pressure from 1 to 210 bar.

Scaling analysis considers two extreme cases. In the first one, most of the heat lost by the wire is used to heat the water while, in the second one, it is used for vaporization. As the majority of the tests correspond to the first case, a correlation is established for these cases of high subcooling. Differences with other similar type correlations are discussed and explained by different film boiling configurations.

1. Introduction

When a hot liquid comes into contact with a colder more volatile one, we may observe what is called a vapor explosion [1]. This phenomenon results from the fine fragmentation of the hot liquid (fragment size ~100 μm) inducing an intense vapor production due to the increase of interfacial area and the increase of heat transfer intensity linked with the small size of the fragments.

In this paper this heat transfer is studied through the analysis of the TREPAM experiment. TREPAM investigates the cooling of a very hot (T_w from 1350 to 2900 K) thin tungsten wire (D from 10 to 250 μm) subjected to a water flow at constant velocity (U_∞ from 0.2 to 46 m/s) with a subcooling ΔT_∞ from 0 to 350 K and under a pressure P_∞ from 1 to 210 bar.

Similar experiments have already been performed by Honda et al. [2] and Inoue et al. [3] using platinum wires but at lower temperatures and under atmospheric pressure. In these previous experiments, film boiling heat fluxes as high as 20 MW/m^2 were observed during several ms. As for the influence of the different parameters, it was found that the film boiling heat fluxes increase with subcooling and relative velocity and when the wire diameter is reduced. They are also quite independent of the wire temperature.

2. Experimental apparatus and method

The experimental device is shown in Fig. 1. It is located into a small cylindrical vessel ($d = 6.3$ cm; $h = 30$ cm) which can stand pressure up to 25 MPa and can be heated up to 650 K. The pressure is imposed by argon injection and the desired ambient temperature is obtained by heating all the test section.

In this cell are located the filament which is electrically heated to the desired temperature and whose resistance variation will be used to determine the heat transferred to water and a small water pool ($d = 3$ cm, $h = 6$ cm) which can be pushed upward at

* Corresponding author. Tel.: +33 438783244.
E-mail address: georges.berthoud@cea.fr (G. Berthoud).

1290-0729/$ – see front matter © 2009 Elsevier Masson SAS. All rights reserved.
doi:10.1016/j.ijthermalsci.2009.01.012

Nomenclature

C_p	heat capacity
D	diameter
h	heat transfer coefficient
L	latent heat of evaporation
Nu	Nusselt number
P	pressure
Pr	Prandtl number
q	heat flux
R	radius
Re	Reynolds number
Sc	subcooling number ($= \frac{C_{pL}\Delta T_L}{L\mathrm{Pr}_L}$)
Sp	superheat number ($= \frac{C_{pV}\Delta T_V}{L\mathrm{Pr}_V}$)
T	temperature
u,v	axial and transverse velocities
U_∞	bulk liquid velocity

Greek symbols

α	thermal diffusivity
β	$\beta \triangleq (\frac{\nu_V}{\nu_L})^{1/2}(\frac{\rho_V}{\rho_L})^{1/4}$
δ_V	vapor film thickness
δ_L^H	hydrodynamic boundary layer thickness
δ_L^T	thermal boundary layer thickness
ε	$\varepsilon \triangleq (\frac{\rho_V}{\rho_L})^{\frac{1}{2}}$
μ	dynamic viscosity
ν	kinematic viscosity
ρ	density

Subscripts

L	liquid
V	vapor
W	wire
i	vapor–liquid interface
exp	experimental
IS	Ito–Shigeshi
EH	Epstein–Hauser
peak	peak heat flux condition
sat	saturation condition
∞	bulk liquid condition

a prescribed and measured velocity through a transient magnetic field applied to a piston rod linked to the water pool.

As shown in Fig. 2, the thin tungsten wire is welded to two electrodes. These electrodes are used to bring the high intensity current for heating the wire, to bring the low intensity current to measure the filament resistance during the quenching phase (through voltage measurement) and to hold the wire horizontally. It also shows that, in the early times of the experiment, heat transfer is uniform along the wire and that the cooling effect of the electrodes is negligible.

The experimental sequence is the following. First, the test section is heated to the desired initial water temperature and pressurized to the desired pressure. Then the upward motion of the water is launched and, at about 2 ms before water–wire contact, the wire is rapidly heated – in less than 800 μs in order to avoid oxidation of the wire – by a high intensity current produced by a high capacity discharge. Then, heating is switched off and an imposed and measured low intensity current is sent to the wire. Measurement of the drop voltage through the wire allows to calculate the wire resistivity variation, so the wire temperature evolution and to deduce the heat flux transferred to water.

Assuming (in fact we checked it) that the wire temperature is uniform radially and axially, we have:

$$q = \rho_W \frac{V}{S}\frac{dH}{dt} = \rho_W \frac{V}{S}\frac{dH}{dT_W}\frac{dT_W}{dt}$$

where ρ_W, V, S are the wire density, volume and cross section and H (T_W), the specific enthalpy, comes the equation of state of the wire material (tungsten) while (dT_W/dt) is obtained through a statistical line fitting the temporal evolution of the wire temperature.

The uncertainty of the measured heat flux q is estimated to be of the order of ±20%.

3. Typical results and control parameters influence

All the results are similar to the one presented in Fig. 3 where we see:

For a short period before the beginning of wire immersion ($t < t_i$), the wire is cooled by the argon forced convection due to the water motion.

Then the heat flux starts to rise when the wire penetrates through the water (the impact time is visible through the slope change on the T_W curve) reaching a maximum shortly after full immersion of the wire into the water.

Then it decreases almost linearly for some ms (about 2 ms for this test). As the temperature decrease is also almost linear, the heat transfer coefficient defined as

$$h = \frac{q}{T_W - T_{sat}(P)} \text{ varies also linearly}$$

Then, the wire temperature is no more axially uniform as it is cooled from both ends by the electrodes

So, as the peak heat flux is representative of the quenching, we use it to characterise the influence of the different control parameters which are evaluated for this condition.

An idea of the test reproducibility is given when comparing tests 75 and 77 (see Table 1).

Due to the experimental procedure, it was difficult to vary only one control parameter so the analysis of the parameter influence was not so easy.

3.1. Wire and water temperatures

As it can be seen from the results of tests 40, 42, 45 and 46, for a given water temperature, the higher the wire temperature, the higher the heat flux (40–42; 45–46) and the heat flux increase is higher when subcooling decreases (see Table 1).

3.2. Wire diameter and relative velocity

As expected, when the wire diameter decreases (12–4/57–64) or when the relative velocity increases (59–40/60–36), the heat flux increases (see Table 1)

We must note that all these tests are highly subcooled

3.3. Ambient pressure

It is very difficult to assess due to the difficulty to find tests in which only the ambient pressure was varied. But, comparing test 4–15–21 and 16 it is found that there is not a big effect of the pressure between 10 and 20 MPa.

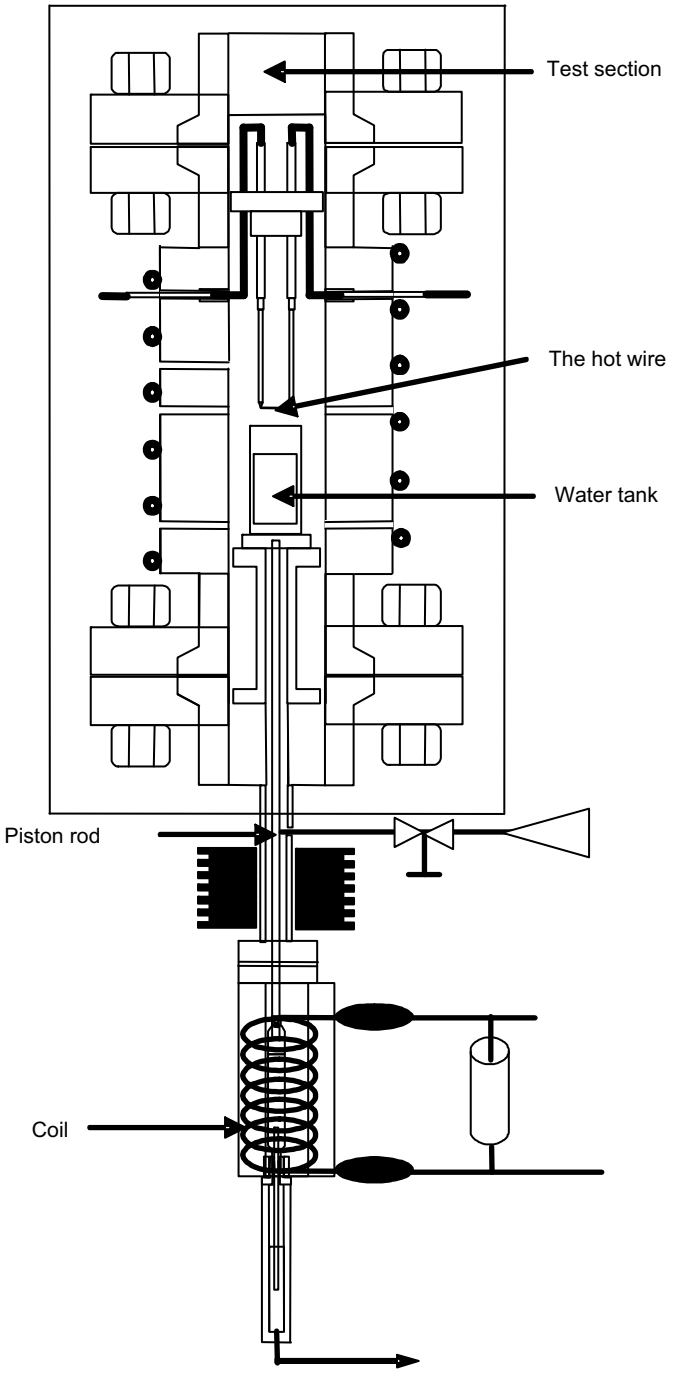

Fig. 1. Schematic of the TREPAM test section.

Then comparing tests 2–10–9–8 and 5, it seems that the influence of the pressure is only sensible at pressure under 0.5 MPa (see Table 2)

Once again, all these tests are highly subcooled.

4. Analysis

4.1. Methodology

First, we try to correlate the heat flux lost by the wire (at the peak) as a function of the control parameters:

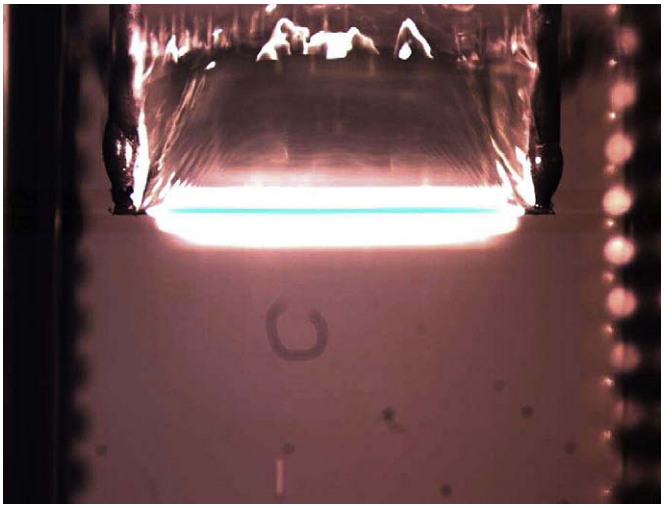

Fig. 2. The tungsten wire during quenching.

- the wire diameter D or radius R
- the wire temperature T_w or wire superheat $\Delta T_V = T_w - T_{sat}$
- the water temperature T_∞ or water subcooling $\Delta T_L = T_{sat} - T_\infty$
- the pressure P_∞
- the bulk liquid velocity U_∞

Concerning the existence of direct contacts between the wire and the liquid coolant, we suppose that, due to the very high wire temperatures, a vapor film exists since the impact of the coolant on the wire. This is confirmed by the measured values of the heat transfer coefficients at the peak heat flux which are much lower than those observed by Inoue et al. [3] in tests about the collapse of a vapor film by a pressure pulse ($h \approx 10^5$ W/m^2 K for smaller superheats). Such contacts have been used by Honda et al. [2] to explain some high measured heat fluxes in their experiments which are performed at smaller wire superheats. If we estimate the vapor film thicknesses by $\delta_V \approx \lambda_V(\Delta T_v/q_{peak})$, we got values varying from 2.3 to 25 μm for Honda et al. while varying from 6.1 to 33.4 μm in TREPAM at 1 bar. So, direct contacts are more difficult to get in TREPAM. That means that, even if some direct contacts occur, they are not significant on the heat exchange because they happen on a very short time. In fact, we do not see them on the resulting graphics. As a conclusion, we consider a film boiling heat transfer in our study.

In order to establish a correlation providing a Nusselt number at peak head flux i.e.:

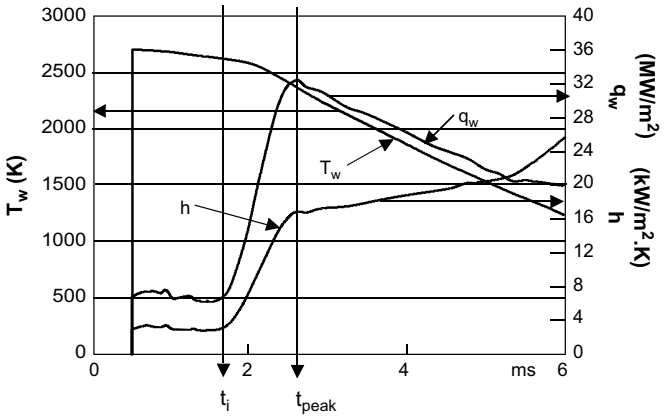

Fig. 3. Typical TREPAM results: evolution of wire temperature T_w (K), heat flux density q_W (MW/m^2) and heat transfer coefficient h (kW/m^2 K) for test T71.

$Nu_{D,peak} \triangleq \frac{q_{peak}D}{\Delta T_{Vpeak}\lambda_V}$, we choose to scale a simplified film boiling model in order to get proper non dimensional numbers.

4.2. The simplified physical model

We consider a stationary cylinder of radius R in an upward flowing liquid at constant velocity U_∞. x is the arc length measured from the stagnation point and y the coordinate normal to the cylinder surface. Around the vapor film of thickness δ_V there is a thin liquid region where velocity and temperature vary, so we will use the classical boundary layer approximations, and if the vapor film and liquid boundary thicknesses (hydrodynamic δ_L^H and thermal δ_L^T) are small compared to the cylinder radius, the cylinder can be dealt as a plane. If we neglect the temporal variation of the wire temperature during the characteristic convection time (D/U_∞), the boundary conditions do not vary with time after full immersion of the wire, so the problem can be considered as quasi-steady i.e. $(\partial/\partial t) = 0$.

Other assumptions are:

- the vapor and liquid flows are laminar (Re_L and $Re_V < 3.10^5$)
- the wire temperature T_w is uniform: no axial conduction effect due to the colder electrodes (we restrict the study to such time scales) and no radial temperature profile (the maximum value of the Biot number is around one percent)
- gravitational forces are negligible (the Froude numbers in the vapor and liquid flows are large compared to 1)
- due to the low value of tungsten emissivity, radiation heat transfer is neglected: the radiative contribution is at maximum 5% of the measured heat flux.
- the vapor–liquid interface is smooth and at saturation
- the physical properties of vapor and liquid are constant and uniform, evaluated at "film" temperature i.e. at $(T_w + T_{sat})/2$ for vapor and $(T_{sat} + T_\infty)/2$ for the liquid. According to Cess and Sparrow [5], this is a good approximation if the vapor properties are such that $\rho\mu = \text{constant}$, $\rho\lambda = \text{constant}$ and $Pr = \text{constant}$ which is about the case for water at low pressure.
- the vapor flow is incompressible

Under these hypotheses the basic conservation equations are the following:

- outside the liquid boundary layer ($y \geq \delta_V + \delta_L$), the liquid temperature is T_∞ and its velocity is given by the potential theory i.e. $u_L \cong (2U_\infty/R)x_L$ while $P_L + (1/2)\rho_L u_L^2$ is constant [4].
- in the liquid boundary layer, the continuity, momentum and energy equations are:

$$\frac{\partial u_L}{\partial x_L} + \frac{\partial v_L}{\partial y_L} = 0 \tag{1}$$

$$u_L\frac{\partial u_L}{\partial x_L} + v_L\frac{\partial u_L}{\partial y_L} = -\frac{1}{\rho_L}\frac{dP_L}{dx_L} + \nu_L\frac{\partial^2 u_L}{\partial y_L^2} \tag{2}$$

and the pressure continuity across the boundary layer $(\partial P/\partial y = 0)$ yields $(dP_L/dx_L) = (dP_L/dx_L)(y = \delta_V + \delta_L) = -4\rho_L U_\infty^2 (x_L/R)$

$$u_L\frac{\partial T_L}{\partial x_L} + v_L\frac{\partial T_L}{\partial y_L} = \alpha_L\frac{\partial^2 T_L}{\partial y_L^2} \tag{3}$$

- at the vapor–liquid interface, the velocity, shear stress and mass continuity provide:

Table 1
Effect of wire temperature, water temperature, wire diameter and relative velocity on TREPAM heat fluxes.

Test number	$T_{w,\,peak}$ (K)	T_∞ (K)	P_∞ (bar)	U_∞ (m/s)	D (μm)	q_{peak} (MW/m²)
40	**1695**	**290**	1.2	2	231	11
45	**1695**	**365**	1.2	2	238.6	4.2
42	**2620**	**297**	1.2	2	234.5	14.9
46	**2700**	**363**	1.2	2	237.2	12
12	2700	293	1	1.8	**238**	17.3
4	2780	293	1	1.6	**95.7**	28.7
57	1350	293	1.2	0.2	**232.8**	5.4
64	1280	301	1.2	0.2	**23.8**	10.9
59	1840	297	1.2	**0.2**	242.1	6.8
40	1695	290	1.2	**2**	231	11
60	1630	297	1.2	**0.2**	47.5	8.7
36	1520	297	1.2	**2**	46.6	16.1

$$u_{Vi} = u_{Li} \tag{4}$$

$$\mu_L\left.\frac{\partial u_L}{\partial y_L}\right|_i = \mu_V\left.\frac{\partial u_V}{\partial y_V}\right|_i \tag{5}$$

$$\dot{m}_V = \rho_V v_{Vi} = \rho_L v_{Li} \tag{6}$$

while temperature and energy balance give:

$$T_{Li} = T_{Vi} = T_{sat}(P_\infty) \tag{7}$$

$$-\lambda_V\left.\frac{\partial T_V}{\partial y}\right|_i + \lambda_L\left.\frac{\partial T_L}{\partial y}\right|_i = \rho_V v_{Vi} L \tag{8}$$

in the vapor film, the mass, momentum and energy balances read:

$$\frac{\partial u_V}{\partial x_V} + \frac{\partial v_V}{\partial y_V} = 0 \tag{9}$$

$$u_V\frac{\partial u_V}{\partial x_V} + v_V\frac{\partial u_V}{\partial y_V} = -\frac{1}{\rho_V}\frac{dP_V}{dx_V} + \nu_V\frac{\partial^2 u_V}{\partial y_V^2} \tag{10}$$

and the pressure continuity across the boundary layer $(\partial P/\partial y = 0)$ yields $(dP_V/dx_V) = (dP_L/dx_L) = -4\rho_L U_\infty^2 (x_L/R)$

$$u_V\frac{\partial T_V}{\partial x_V} + v_V\frac{\partial T_V}{\partial y_V} = \alpha_V\frac{\partial^2 T_V}{\partial y_V^2} \tag{11}$$

4.3. Scaling analysis

4.3.1. Scaling analysis for highly subcooled conditions (case 1)

In this case of high subcooling, as vaporization is weak, it is expected that the longitudinal velocity in the vapor film is of the order of the velocity in the liquid boundary layer and that heat is

Table 2
Effect of ambient pressure on TREPAM heat fluxes.

Test number	$T_{w,\,peak}$ (K)	T_∞ (K)	P_∞ (bar)	U_∞ (m/s)	D (μm)	q_{peak} (MW/m²)
4	2780	293	**1**	1.6	95.7	28.7
15	2860	293	**100**	1.5	87.3	48
21	2550	293	**150**	1.3	94.5	48
16	2350	293	**200**	1.1	87.2	46.5
2	2350	293	**1**	1.7	233	15
10	2550	293	**5**	1.6	234.4	23
9	2585	293	**10**	1.6	235.1	25.6
8	2470	293	**25**	1.6	237.3	26
5	2220	293	**50**	1.6	229.4	25

Table 3
TREPAM test conditions and results (For interpretation of color in this table the reader is referred to the web version of the article.).

test number	P bar	D μm	U_∞ m/s	T_w K	ΔT_V K	T_∞ K	ΔT_L K	q_{peak}	h kW/m^2.K	Nu_{exp}	A	B
25	1	236	1.3	2550	2177	293	80	14.7	6.8	9.72	100.0	1.34
2	1	233	1.7	2530	2157	293	80	15	7.0	9.94	100.9	1.35
12	1	238	1.8	2700	2327	293	80	17.3	7.4	10.05	91.7	1.26
75	1	232	11.5	2375	2002	293	80	26.3	13.1	20.22	110.9	1.44
77	1	232	11	2400	2027	293	80	27	13.3	20.22	109.3	1.43
78	1	237	21.4	2350	1977	293	80	40	20.2	32.19	112.9	1.46
76	1	229	22.7	2270	1897	293	80	35	18.5	29.58	119.1	1.51
79	1	229	46	2270	1897	293	80	58.1	30.6	49.15	119.1	1.51
1	1	96	2	2460	2087	293	80	24	11.5	6.97	105.0	1.39
3	1	95	1.7	2150	1777	293	80	17.5	9.8	6.90	128.5	1.59
4	1	96	1.6	2780	2407	293	80	28.7	11.9	6.27	87.9	1.23
26	1	47	2.3	2800	2427	293	80	35.5	14.6	3.70	86.8	1.22
28	1	9	2.2	2100	1727	293	80	35	20.3	1.38	133.6	1.63
29	1	9	2.2	2000	1627	293	80	36	22.1	1.54	143.7	1.72
27	1	9	2.2	1800	1427	293	80	26	18.2	1.47	170.6	1.93
57	1.2	233	0.2	1350	972	293	85	5.4	5.6	16.43	264.5	2.68
58	1.2	238	0.2	2300	1922	293	85	8.3	4.3	7.05	111.8	1.51
59	1.2	242	0.2	1840	1462	297	81	6.8	4.7	10.05	145.9	1.84
40	1.2	231	2	1695	1317	290	88	11	8.4	18.91	192.5	2.15
42	1.2	234	2	2620	2242	297	81	14.9	6.6	9.17	84.8	1.28
45	1.2	239	2	1695	1317	365	13	4.2	3.2	7.46	5.0	0.38
46	1.2	237	2	2700	2322	363	15	12	5.2	6.93	3.3	0.27
55	1.2	99	2	1900	1522	361	17	9	5.9	5.00	7.1	0.43
53	1.2	100	2	1780	1402	294	84	13.9	9.9	9.18	164.1	1.97
54	1.2	96	2	2300	1922	293	85	18	9.4	6.14	111.8	1.51
61	1.2	47	0.2	2300	1922	303	75	16	8.3	2.66	89.9	1.37
60	1.2	48	0.2	1630	1252	297	81	8.7	6.9	3.37	176.3	2.09
63	1.2	45	0.2	1620	1242	358	20	8.5	6.8	3.20	12.7	0.60
62	1.2	45	0.2	1380	1002	338	40	6	6.0	3.33	63.6	1.38
48	1.2	38	2	2130	1752	291	87	24	13.7	3.84	130.3	1.66
51	1.2	36	2	1920	1542	361	17	13.7	8.9	2.71	7.0	0.43
36	1.2	47	2	1520	1142	297	81	16.1	14.1	7.30	198.9	2.27
50	1.2	39	2	1525	1147	360	18	10.4	9.1	3.97	11.5	0.58
65	1.2	23	0.2	1800	1422	301	77	14.5	10.2	2.17	137.4	1.81
64	1.2	24	0.2	1280	902	301	77	10.9	12.1	3.89	244.9	2.65
10	5	234	1.6	2550	2125	293	132	23	10.8	15.10	68.4	1.53
72	6	46	1.5	1980	1548	432	0	20.6	13.3	4.77	-	-
66	10	228	1.2	2660	2207	453	0	14.9	6.8	8.60	-	-
67	10	222	1.4	2500	2047	383	70	15.1	7.4	9.80	12.4	0.81
68	10	219	1.4	2515	2062	338	115	18.3	8.9	11.59	31.7	1.25
9	10	235	1.6	2585	2132	293	160	25.6	12.0	16.32	55.1	1.57
69	10	93	1.6	2330	1877	434	19	20	10.7	6.46	1.0	0.25
70	10	93	2	2500	2047	453	0	22.4	10.9	6.11	-	-
71	10	95	2	2400	1947	293	160	32	16.4	10.02	61.9	1.70
8	25	237	1.6	2470	1973	293	204	26	13.2	18.61	45.6	1.73
73	30	46	2	1840	1333	507	0	21.3	16.0	5.98	-	-
74	42	228	1.8	2540	2014	526	0	15.4	7.6	9.95	-	-
5	50	229	1.6	2220	1683	293	244	25	14.9	22.27	45.6	2.03
19	50	93	1.9	2620	2083	293	244	48	23.0	11.83	35.8	1.71
20	50	46	1.9	2450	1913	293	244	65	34.0	9.30	39.4	1.83
7	75	228	1.4	2320	1756	293	271	25.7	14.6	20.64	40.5	2.02
6	100	227	1.4	2170	1586	293	291	24.4	15.4	22.63	44.1	2.25
15	100	87	1.5	2860	2276	293	291	48	21.1	9.20	29.8	1.71
11	150	234	1.1	2360	1744	293	323	28.3	16.2	22.51	43.4	2.27
21	150	95	1.3	2550	1934	293	323	48	24.8	12.96	39.0	2.10
33	160	47	1.4	2700	2079	293	328	68	32.7	8.05	37.9	2.05
22	200	230	1.2	2100	1461	293	346	24	16.4	24.23	76.4	3.03
16	200	87	1.1	2350	1711	293	346	46.5	27.2	13.86	65.3	2.71
30	200	46	1.2	1650	1011	293	346	60	59.3	21.05	109.4	3.89
17	210	95	1.2	1950	1307	293	350	43.3	33.1	21.17	106.5	3.53

just conducted through it to the interface (no influence of convection). The drag imposed by the liquid forces the flow of vapor from the stagnation point to the rear. In the limit of high subcooling, the vapor layer does not separate and the effect of convection is simply to redistribute the heat flux. In other words, the vapor flow adapts itself to the liquid flow.

So, in the liquid boundary layers, scales are defined as in the classical boundary layer theory i.e.

$L_{Lx1} \sim R$

$u_{L1} \sim U_\infty$ (characteristic velocity of the external flow which varies from 0 at the stagnation to $2U_\infty$ at the equator). This scale is valid for the hydrodynamic and thermal boundary layers. Then:

$$\delta_{L1}^{H} \sim R\mathrm{Re}_{L1}^{-1/2} \text{ with } \mathrm{Re}_{L1} \triangleq \frac{U_\infty R}{\nu_L}$$

$$\delta_{L1}^{T} \sim R\mathrm{Re}_{L1}^{-1/2}\mathrm{Pr}_L^{-1/2}$$

$$v_{L1} \sim U_\infty \mathrm{Re}_{L1}^{-1/2} \text{ (from the continuity equation (1))}$$

As for the vapor film, as its behaviour is governed by heat conduction, its thickness δ_{v1} is evaluated from the interfacial energy balance for case 1 i.e.:

$$\lambda_V \frac{\Delta T v}{\delta_{V1}} \sim \lambda_L \frac{\Delta T_L}{\delta_{L1}^{T}} \text{ with } \Delta T_V = T_w - T_{sat}$$

Then

$$\begin{aligned}\delta_{V1} \sim \frac{\lambda_V \Delta T_V}{\lambda_L \Delta T_L} R\mathrm{Re}_{L1}^{-1/2}\mathrm{Pr}^{-1/2} &= \frac{\nu_V \rho_V C_{pV} \Delta T_V \mathrm{Pr}_L}{\nu_L \rho_L C_{pL} \Delta T_L \mathrm{Pr}_V} R\mathrm{Re}_{L1}^{-1/2}\mathrm{Pr}_L^{-1/2} \\ &= \frac{\nu_V \rho_V}{\nu_L \rho_L} \frac{\mathrm{Sp}}{\mathrm{Sc}} R\mathrm{Re}_{L1}^{-1/2}\mathrm{Pr}_L^{-1/2} \\ &= \left(\frac{\mu_V}{\mu_L}\right)\frac{\mathrm{Sp}}{\mathrm{Sc}} R\mathrm{Re}_L^{-1/2}\mathrm{Pr}_L^{-1/2}\end{aligned}$$

This expression for the vapor film thickness explains why the film boiling correlations of Epstein–Hauser [6], and Ito et al. [7,8] for large subcoolings are expressed as:

$$\mathrm{Nu} = C\left(\frac{\mu_L}{\mu_V}\right)\frac{\mathrm{Sc}}{\mathrm{Sp}}\mathrm{Re}_L^{1/2}\mathrm{Pr}_L^{1/2}$$

Using the variables defined by Epstein–Hauser [6]:

$$\beta \triangleq \left(\frac{\nu_V}{\nu_L}\right)^{1/2}\left(\frac{\rho_V}{\rho_L}\right)^{1/4}; \quad \varepsilon \triangleq \left(\frac{\rho_V}{\rho_L}\right)^{\frac{1}{2}}; \quad \mathrm{Sp} \triangleq \frac{C_{pV}\Delta T_V}{L\mathrm{Pr}_V}; \quad \mathrm{Sc} \triangleq \frac{C_{pL}\Delta T_L}{L\mathrm{Pr}_L}$$

it comes $\delta_{V1} \sim \beta^2 \varepsilon (\mathrm{Sp}/\mathrm{Sc}) R\mathrm{Re}_{L1}^{-1/2}\mathrm{Pr}_L^{-1/2}$

As already mentioned, the longitudinal velocity in the vapor is of the order of the liquid one:

$$u_{V1} \sim u_{L1} \sim U_\infty$$

Then, using the continuity equation (9) and $L_{VX1} \sim R$, we have:

$$v_{V1} \sim \beta^2 \varepsilon \frac{\mathrm{Sp}}{\mathrm{Sc}} U_\infty \mathrm{Re}_{L1}^{-1/2}\mathrm{Pr}_L^{-1/2}$$

As for the pressure, we have:

$$\left.\frac{dP_V}{dx}\right|_{scale} = \left.\frac{dP_L}{dx}\right|_{scale} \sim 4\rho_L \frac{U_\infty^2}{R} \text{ (boundary layer approximation)}$$

4.3.2. Scaling analysis for small subcooling conditions (case 2)

In this case of small subcooling, we consider that the longitudinal velocities in the vapor film are large compared to the liquid ones due to the important vaporization. That means that the liquid flow is governed by the vapor flow: the liquid is dragged upward by the vapor flow. This vapor flow is more governed by the pressure gradient from the external flow: vapor will flow from both front and rear stagnation points towards the equator and separation in the vapor film may occur.

So we chose to use as a longitudinal velocity scale u_{v2} of the order of the mean velocity of a Poiseuille flow between two planes distant of δ_V under the previous mentioned pressure gradient i.e.

$$u_{V2} = \frac{\rho_L}{3\mu_V}\delta_{V2}^2 \frac{U_\infty^2}{R}$$

Then, from the continuity equation we have:

$$\frac{u_{V2}}{R} \sim \frac{v_{V2}}{\delta_{V2}}$$

and from the approximate energy balance at the interface (8):

$$\rho_V v_{V2} L \sim \lambda_V \frac{\Delta T_V}{\delta_{V2}}$$

These 3 equations with 3 unknowns u_{v2}, v_{v2} and δ_{v2} give:

$$u_{V2} \sim \left[\frac{\rho_L}{\rho_V}\frac{\lambda_V \Delta T_V}{3\mu_V L}U_\infty^2\right]^{1/2} \sim \frac{1}{\sqrt{3}}\frac{U_\infty}{\varepsilon}\mathrm{Sp}^{1/2} \quad \text{then } \mathrm{Re}_{V2} = \frac{RU_\infty \mathrm{Sp}^{1/2}}{\sqrt{3}\varepsilon \upsilon_V}$$

$$\delta_{V2} \sim \mathrm{Sp}^{1/2} R\mathrm{Re}_{V2}^{-1/2} \tag{12}$$

$$v_{V2} \sim \frac{\mathrm{Sp}\mathrm{Re}_{V2}^{-1/2}}{\varepsilon\sqrt{3}}U_\infty$$

NB: In order to check these evaluations, we can compare them to the results of a more elaborated model by Ito et al. [7] who found for saturated water and $\mathrm{Fr} = 50$, $\mathrm{Sp} = 1$ at the stagnation point ($y = 0$ their Fig. 2) that $u_{Vmax} \approx 10u_i = 10(u_{Lext}/0.4) = 10\,(2U_\infty/0.4) \sim 50U_\infty$

Using equation (12), we get $u_{V2} \sim 35\ U_\infty$ which is a good estimation.

To get scales in the liquid phase, we use the fact that the liquid boundary layer results from the drag exerted by the vapor flow. So we use the fact that the inertial terms are of the order of the viscous ones in the momentum equation (2) and the shear stress continuity (5):

$$\frac{u_{L2}^2}{R} \sim \nu_L \frac{u_{L2}}{\delta_{L2}^{H}}$$

$$\mu_V \frac{u_{V2}}{\delta_{V2}} \sim \mu_L \frac{u_{L2}}{\delta_{L2}^{H}}$$

That gives:

$$u_{L2} = \left(\frac{\rho_V \mu_V}{\rho_L \mu_L}\right)^{1/3}\mathrm{Sp}^{1/6}\frac{U_\infty}{\varepsilon\sqrt{3}} = \frac{\beta^{2/3}\mathrm{Sp}^{1/6}}{\sqrt{3}}U_\infty$$

$$\delta_{L2}^{H} = R\mathrm{Re}_{L2}^{-1/2} \text{ with } \mathrm{Re}_{L2} \triangleq \frac{u_{L2}R}{\nu_L} = \left(\frac{\rho_V \mu_V}{\rho_L \mu_L}\right)^{1/3}\frac{\mathrm{Sp}^{1/6}}{\varepsilon\sqrt{3}}\frac{U_\infty R}{\nu_L}$$

and, as for case 1, $\delta_{L2}^{T} \sim \delta_{L2}^{H}\mathrm{Pr}_L^{-1/2}$

4.3.3. Criteria for case selection

In order to get criteria for case selection, we compare the contribution of liquid heating (Φ_L) and vaporization (Φ_V) in the interfacial energy balance (8) with the scales defined for the two extreme cases, i.e.:

- for case 1

$$A \triangleq \frac{0(\text{liquid heating})}{0(\text{vaporization})} = \frac{\Phi_{L1}}{\Phi_{V1}} = \frac{\frac{\lambda_L \Delta T_L}{\delta_{L1}^{T}}}{\rho_V v_{V1} L} = \frac{\mathrm{Sc}^2}{\mathrm{Sp}}\frac{1}{\beta^2\varepsilon^3}\mathrm{Pr}_L \gg 1$$

- for case 2

$$B \triangleq \frac{0(\text{liquid heating})}{0(\text{vaporization})} = \frac{\Phi_{L2}}{\Phi_{V2}} = \frac{\frac{\lambda_L \Delta T_L}{\delta^+_{L2}}}{\rho_V \nu_{V2} L} = \frac{Sc}{Sp^{2/3}} \frac{1}{(\beta^2 \varepsilon^3)^{1/3}} Pr_L^{1/3} \ll 1$$

These numbers are shown for all the Trepam tests in Table 3. According to these criteria, we found:

- 47 tests with $A \gg 1$: 29.8 (T15 very high superheat) $\leq A \leq$ 264.5 (T57, low superheat, large subcooling) while B not $\ll$1. They are shown in green for the tests where the heat transfer coefficient is seen to increase during quenching as shown Fig. 3 and in red for the tests where the heat transfer coefficient decreases slightly during quenching as shown Fig. 6 for test T1.
- 5 saturated tests (in blue) with $B = 0$
- 8 intermediate tests (in white) in which:
  (T46 with $B = 0.27$) $3.3 \leq A \leq 12.7$ (T63 with $B = 0.6$)
  (T46) $0.27 \leq B \leq 0.81$ (T67 with $A = 12.4$)

One can check this simplified analysis by comparing the estimation of the heat flux i.e. $q \approx \Phi_{L1} = \frac{\lambda_L \Delta T_L}{\delta^+_{L1}}$ for case 1 tests and $q \approx \Phi_{V2} = \rho_V \nu_{V2} L$ for case 2 tests. Such results are presented in Table 4 for case 1 and in Table 5 for case 2.

If we take out the 10 μm diameter tests (27, 28, 29) which obviously do not satisfy the boundary layer hypothesis ($\delta_V \ll R$), we found for case 1 tests:

$$(\text{T59} : 1\ \text{bar}; 0.2\ \text{m/s}) \quad 0.6 \langle \frac{\Phi_{L1}}{q_{exp}} \langle 2.4 \quad (\text{T22}; 200\ \text{b}; 1.2\ \text{m/s})$$

and for the five saturated cases:

$$(\text{T66} - 10\text{b}) \quad 1.2 \langle \frac{\Phi_{V2}}{q_{exp}} \langle 1.8 \quad (\text{T73} - 30\text{b})$$

which is satisfying.

As for the so-called intermediate tests, it appears (see Table 6) that, even it has been postulated that $\phi_{L1} \gg \phi_{V1}$ for getting case 1 scales and that $\phi_{V2} \gg \phi_{L2}$ for getting case 2 scales, it is not exactly the case which confirms that these tests are really intermediate.

Table 5
Comparison of the estimated heat flux (from the scaling analysis) to the experimental one for TREPAM case 2 tests (saturated tests).

Test number	ϕ_{v2} (MW/m^2)	q_{exp}	ϕ_{V2}/q_{exp}
77	26.5	20.6	1.29
66	17.7	14.9	1.19
70	32.9	22.4	1.47
73	37.9	21.3	1.78
74	26.8	15.4	1.74

However, keeping in mind that the experimental heat flux is known at ±20%, tests 45–55–51–50 and 67 can be said close to case 1: the relative "error" is between −10% and −35% while tests 46 and 63 are close to case 2 and 69 can be said in between ($A \sim B$).

At this time, it is necessary to recall that, for case 1 tests, the simplified analysis does not take into account:

- the effect of the wire temperature on the heat flux (see for example tests 40/42 results in Section 3.1) which does not appear in the convective heat flux φ_{L1} which is independent of T_w
- the effect of the pressure (levelling effect at high pressure) which is not found as strong with φ_{L1} evaluation as it is observed experimentally as we can see when comparing φ_{L1} evaluation for the tests 2/10/9/8/5 referred in Section 3.3 (see Table 7)

This discrepancy can be attributed to the rough estimation of the liquid boundary layer scales which are the ones for an external flow (U_∞) along a plate while, in the actual situation, the velocity profiles are such that the velocity in the vapor film is slightly higher than the external one. So the velocity difference to take into account in the liquid boundary layer is rather Ui–U_∞. As it is expected that, due to the change in the vapor density, the drag exerted by the vapor flow on the liquid will decrease when the pressure increases, Ui/U_∞ will decrease when the pressure increases. This will lead to larger liquid boundary layers at high pressure which will decrease the heat flux evaluation.

In fact, such a behaviour is observed when looking at the results of more detailed film boiling models like the one of Boulin [9] who

Table 4
Comparison of the estimated heat flux (from the scaling analysis) to the experimental one for TREPAM case 1 tests (high subcooling).

Test number	ϕ_{L1} (MW/m^2)	q_{exp}	ϕ_{L1}/q_{exp}	Test number	ϕ_{L1}	q_{exp}	ϕ_{L1}/q_{exp}
25	11.5	14.7	0.78	62	5.52	6	0.92
2	13.2	15	0.88	48	38.9	24	1.62
12	13.4	17.3	0.77	36	32.8	16.1	2.04
75	34.4	26.3	1.31	65	14.0	14.5	0.97
77	33.6	27	1.24	64	13.9	10.9	1.27
78	46.5	40	1.16	10	22.6	23	0.98
76	48.7	35	1.39	68	20.3	18.3	1.11
79	69.2	58.1	1.19	9	28.2	25.6	1.10
1	22.3	24	0.93	71	49.7	30.6	1.62
3	20.7	17.5	1.14	8	37.0	26	1.42
4	20.0	28.7	0.70	5	46.0	25	1.84
26	34.4	35.5	0.97	19	78.8	48	1.64
28	76.7	35	2.19	20	111.6	65	1.72
29	78.2	36	2.17	7	48.4	25.7	1.88
27	77.5	26	2.98	6	52.6	24.4	2.15
57	4.85	5.4	0.90	15	87.8	48.0	1.83
58	4.79	8.3	0.58	11	51.3	28.3	1.81
59	4.56	6.8	0.67	21	87.8	48.0	1.79
40	15.9	11	9.44	33	131.7	68.0	1.94
42	14.6	14.9	0.98	22	58.3	24.0	2.42
53	23.2	13.9	1.67	16	90.6	46.5	1.95
54	23.9	18	1.33	30	130.6	60	2.18
61	9.7	16	0.61	17	91.9	43.3	2.12
60	10.3	8.7	1.18				

Table 6
Comparison of the fluxes estimated from the scaling analysis to the experimental ones for the intermediate tests.

Test number	Case 1 flux estimation			q_{exp}	Case 2 flux estimation			$(\phi_{tot1} - q_{exp})/q_{exp}$	$(\phi_{tot2} - q_{exp})/q_{exp}$
	ϕ_{L1}	ϕ_{V1}	ϕ_{tot1}		ϕ_{V2}	ϕ_{L2}	ϕ_{tot2}		
45	2.53	0.50	3.0	4.2	7.5	2.8	10.3	−0.28	+1.45
46	2.92	0.90	3.8	12	14.4	3.8	18.2	−0.68	+0.50
55	5.12	0.72	5.8	9	13.7	6.0	19.7	−0.35	+1.19
63	2.81	0.22	3.0	8.5	5.1	2.8	7.9	−0.55	−0.07
51	8.48	1.21	9.7	13.7	23	9.9	32.9	−0.29	+1.4
50	8.59	0.75	9.3	10.4	15.8	9.3	25.1	−0.10	+1.41
67	12.6	1.1	13.6	15.1	18	14.6	32.6	−0.10	+0.67
69	5.71	5.95	10.2	20	26.8	6.6	33.4	−0.48	+0.67

found from the velocity profiles that $Ui/U_{ext} \sim 2$ for 1 bar tests and 1.25 for test 11 at 150 bar.

The same explanation can be used to explain the effect of the wire temperature on the heat flux (not seen in the simplified analysis as δ_L is independent of T_w) as Ui/U_∞ is expected to increase with T_w (all the other control parameters being kept constant).

4.4. Correlation for highly subcooled tests (case 1)

As the majority of the TREPAM tests correspond to the first case, we can only derive a correlation for such tests. To do so, we use the dimensionless mass, momentum and energy balances of the above simplified model as well as dimensionless boundary conditions, using the case 1 scales defined in 4.3.1. Then, the following non dimensional numbers appear:

Pr_L from the liquid energy balance (3)
Sc/Sp from the shear stress continuity at the V/L interface (5)
$\varepsilon^3\ \beta^2$ Sp/Sc from the interfacial energy balance (8)

We want to correlate the experimental peak heat flux as a function of these numbers. The peak heat flux is scaled by the order of magnitude of the conduction one in the vapor film, i.e.:

$$q^* \triangleq \frac{q_{peak}}{0\left(q_{cond,V}\right)} \text{ with } O\left(q_{cond,V}\right) \sim \frac{\lambda_V \Delta T_V}{\delta_{V1}} = \frac{\lambda_V \Delta T_V}{\beta^2 \varepsilon \frac{Sp}{Sc} R Re_{L1}^{-1/2} Pr_L^{-1/2}}$$

What we finally want is an expression of the Nusselt number at peak value.

$$Nu_{Dpeak} \triangleq \frac{hD}{\lambda_V} = \frac{q_{peak} D}{\lambda_V \Delta T_V} = q^* \frac{\lambda_V \Delta T_V}{\delta_{V1}} \frac{D}{\lambda_V \Delta T_V} = q^* \frac{D}{\delta_{V1}} = \frac{2q^*}{\beta^2 \varepsilon \frac{Sp}{Sc} Re_{L1}^{-1/2} Pr_L^{-1/2}}$$

As we want a correlation for heat transfer governed by external forced convection, we expect to have a dependency of the Nusselt number of the type $Re_L^{1/2}\ Pr_L^{1/2}$. That means that Pr_L should not appear in the correlation for q^*. So we correlate q^* as a function of Sp/Sc and $\varepsilon^3\ \beta^2$ uniquely i.e.:

$$q^* = C\left(\frac{Sp}{Sc}\right)^a \left(\varepsilon^3 \beta^2\right)^b$$

And a least square method provides

$$C = 0.575; \quad a = 0.7 \text{ and } b = 0.21$$

with an absolute percent error of 11% and a root mean square percent error of 14% for the 34 tests verifying the model hypothesis i.e. the boundary layer approximation $(\delta/R \ll 1)$.

From the 47 tests identified as case 1 tests in 4.3.3, the following tests have not been retained:

- the 10 μm diameter tests 27–28–29
- the 0.2 m/s tests: 57–58–59–61–60–62–65–64 (free convection effect)
- plus tests 4 and 26 for which $\delta_{V1}/R \sim 0.5$

That gives for the peak Nusselt number:

$$Nu_{D,peak} = 1.15\left(\frac{Sc}{Sp}\right)^{0.3} \left(\varepsilon^3 \beta^2\right)^{0.21} \left(\beta^2 \varepsilon\right)^{-1} Re_{L1}^{1/2} Pr_L^{1/2}$$

$$Nu_{D,peak} = 1.15\left(\frac{Sc}{Sp}\right)^{0.3} \left(\frac{\rho_V \mu_V}{\rho_L \mu_L}\right)^{0.21} \left(\frac{\mu_L}{\mu_V}\right) Re_{L1}^{1/2} Pr_L^{1/2}$$

with:

$$80 \le Re_{L1} \triangleq \frac{U_\infty R}{\upsilon_L} \le 1.110^4 \quad 1 \le P\infty \le 210 \text{ bar}$$

$$0.92 \le Pr_L \le 3 \quad 50\ \mu m \le D \le 250\ \mu m$$

$$1.7510^{-5} \le \varepsilon^3 \beta^2 = \frac{\rho_V \mu_V}{\rho_L \mu_L} \le 1.2710^{-2} \quad 1,1 \text{ m/s} \le U\infty \le 46 \text{ m/s}$$

$$1520 \text{ K} \le T_w \le 2860 \text{ K} \quad 1140 \text{ K} \le \Delta T_V \le 2302 \text{ K}$$

$$0.08 \le \beta^2 \varepsilon = \frac{\mu_V}{\mu_L} \le 0.41 \quad 0.015 \le \frac{Sc}{Sp} \le 0.55$$

$$80 \text{ K} \le \Delta T\infty \le 350 \text{ K} \quad 273 \text{ K} \le T\infty \le 338 \text{ K}$$

An idea of the precision of the correlation is given in Fig. 4.

This new correlation for *highly subcooled forced convection film boiling* heat transfer around a cylinder can be compared to the ones of

- Epstein–Hauser [6]
$$Nu_{EH} = 2 \times 0.977 \frac{Sc}{Sp} \frac{\mu_L}{\mu_V} Re_L^{1/2} Pr_L^{1/2} (10) \quad (Re_L \triangleq \frac{2RU_\infty}{\nu_L})$$

(NB. the factor 2 was introduced by Epstein–Hauser to "correct" their model when comparing its results to the Motte and Bromley data (ref 1–4 of [6]))

- Shigeshi et al. [8] $Nu_{IS} = 1.15 \frac{Sc}{Sp} \frac{\mu_L}{\mu_V} Re_L^{1/2} Pr_L^{1/2} (Re_L \triangleq \frac{2RU_\infty}{\nu_L})$

who found that the average heat transfer coefficients measured in their experiment were 2 or 3 times as high as their analysis.

A similar behaviour (higher heat transfer than estimated by a film boiling model) was observed by Liu and Theofanous [10]

Table 7
Evolution of the estimated heat flux as a function of the ambient pressure for case 1 tests (large subcooling) compared to the experimental heat flux.

Test number	P (bar)	D (μm)	U_∞ (m/s)	T_W (K)	T_∞ (K)	q_{peak} (MW/m²)	ϕ_{L1} (MW/m²)
2	1	233	1.7	2350	293	15	13.2
10	5	235.4	1.6	2550	–	23	22.6
9	10	235.1	1.6	2585	–	25.6	28.2
8	25	237.3	1.6	2470	–	26	37.0
5	50	229.4	1.6	2220	–	25	46.0

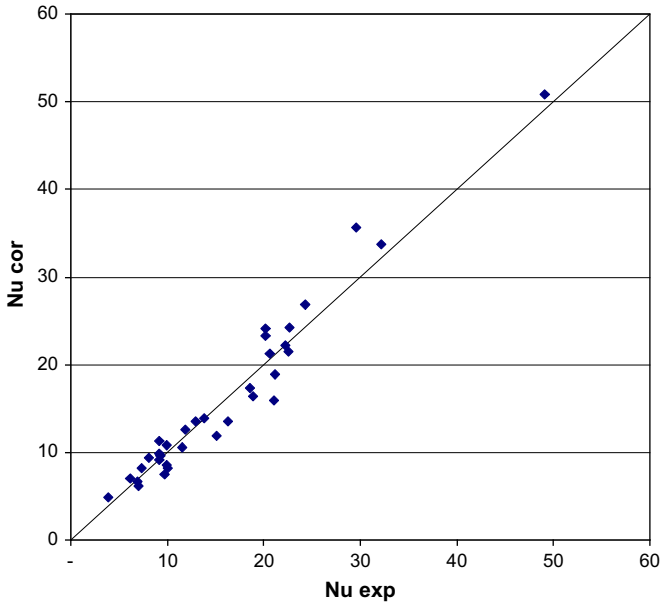

Fig. 4. Comparison of the experimental and correlated Nusselt numbers for the 34 case 1 tests verifying the boundary layer hypothesis.

while modelling highly subcooled forced convection film boiling around spheres at around 1250 K. They found – see their Appendix B – that, in that case:

$$\mathrm{Nu} = C\mathrm{Re}_L^{1/2}\frac{\mu_L}{\mu_V}\frac{\mathrm{Sc}}{\mathrm{Sp}} \quad \text{(B26) with } C = 0.5642 \quad \text{(B27)} \qquad \text{(B26)}$$

but, that the modelled constant is much smaller than the experimental constant of 1.5–2.0 or even more, if we look for example at the result of one their highest temperature subcooled test such as run 10 (page D15 of [10]), where they got $\mathrm{Nu} = 185.4$ ($q_w = 0.95$ MW/m^2) for $P = 1$ b; $D = 12.7$ mm; $T_w = 920$ °C; $T_\infty = 70.9$ °C; $U_\infty = 1.39$ m/s, while the "modelled" Nu by (B26) is 38 which is about 5 times smaller than the experimental one. For this test, our correlation gives $\mathrm{Nu} = 93$ (2 times smaller than the experimental one). It is also interesting to mention that the above "modelled" Nu value (B26) gets closer and closer to the highly subcooled TREPAM results as the pressure increases as it gives:

- for T25 at 1 bar $\mathrm{Nu} = 2$ instead of 9.72 (five times smaller)
- for T8 as 25 bar $\mathrm{Nu} = 9.3$ instead of 18.6 (two times smaller)
- for T22 at 200 bar $\mathrm{Nu} = 23.9$ instead of 24.2

The new correlation introduces a new dimensionless number $\varepsilon^3\beta^2 = (\rho_V\mu_V/\rho_L\mu_L)$. This number can take into account the pressure dependency (through(ρ_V/ρ_L)) which was not assessed in previous experiments, all performed at atmospheric pressure.

Then, the correlation is used for all the tests identified as case 1 or intermediate and the results are shown in Fig. 5.

For the case 1 tests not retained for the correlation:

the error for the 10 μm tests varies between +67% and 100%
the correlation underestimates the heat flux for the 0.2 m/s tests from 33% (T65) to 57% (T57) (free convection effect not taken into account)
the error is -24% for T4 and +7% for T26

As for the "intermediate" tests which looks close to case 1 from the scaling analysis (see Table 4), the correlation is in agreement with the experiment at ±10% while the relative error is −32% for test 46, −34% for test 69 and −57% for test 63 which confirms that the heat transmitted by convection into the liquid is smaller than the heat extracted from the wire: vaporization should play a role.

To compare this new correlation to the correlation of Epstein–Hauser, we must use the full correlation of Epstein–Hauser (eq (45) of their paper) as, according to their criteria:

- when $\frac{B_{EH}}{A_{EH}} \gg 1$, practically all the heat goes into the liquid (i.e. case 1) and formula (10) applies.
- for nearly saturated liquid (i.e. case 2) when $\frac{B_{EH}}{A_{EH}} \ll 1$, vaporization dominates with

$$A_{EH} = \frac{C_{PV}(T_w - T_{SAT})}{\mathrm{Pr}_V L} = \mathrm{Sp}$$

$$B_{EH} = \beta\frac{\lambda_L}{\lambda_V}\frac{C_{PV}(T_{SAT} - T_\infty)}{\mathrm{Pr}_V L}(\mathrm{Pr}_L)^{1/2}$$

For the TREPAM tests designed as case 1, we have $0.4 \le \frac{A_{EH}}{B_{EH}} \le 1.5$. That means that according to their criteria we should have no case 1 test among the TREPAM tests so the full correlation, including both effects, should be used. So

$$\mathrm{Nu}_{EH} = \frac{2.5\mathrm{Re}_L^{1/2}}{\beta}\left[\frac{1}{24A_{EH}} + \left(\frac{2}{\pi}\right)\left(\frac{B_{EH}}{A_{EH}}\right)^4\right]^{0.25} \quad \text{with } \mathrm{Re}_L \triangleq \frac{U_\infty D}{\nu_L}$$

is compared to experimental TREPAM Nusselt numbers and our new correlation in Table 8. For all the case 1 Trepam tests (except T58), the Esptein–Hauser correlation overestimates the heat flux, the over estimation being larger at high pressure, as high as 240% for test 22 at 200 bar.

As for the five saturated TREPAM tests, the Epstein–Hauser also estimates the TREPAM results, the overestimation getting larger as the pressure increases.

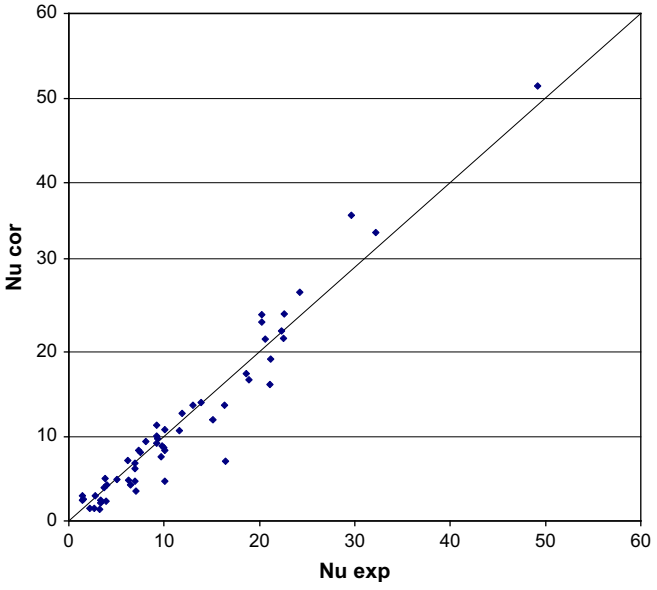

Fig. 5. Comparison of the experimental and correlated Nusselt numbers for all the tests identified as case 1 plus intermediate.

Table 8
Comparison of the new derived correlation to the Epstein–Hauser correlation for the non saturated TREPAM tests.

test number	used for correlating	$\varepsilon^3\beta^2$	$\beta^2\varepsilon$	Sc/Sp	Re_{L1}	Pr_L	Nu_{exp}	Nu_{correl}	Correl Error	$Nu_{EpsteinHauser}$	E H Error
25	yes	1.75E-05	0.12	1.70E-02	3.23E+02	2.99	9.72	7.56	-29%	13.14	35%
2	yes	1.75E-05	0.12	1.71E-02	4.17E+02	2.99	9.94	8.66	-15%	15.15	52%
12	yes	1.74E-05	0.12	1.55E-02	4.51E+02	2.99	10.05	8.29	-21%	13.65	36%
75	yes	1.76E-05	0.11	1.90E-02	2.81E+03	2.99	20.22	24.40	17%	45.48	125%
77	yes	1.76E-05	0.11	1.86E-02	2.69E+03	2.99	20.22	23.53	14%	43.39	115%
78	yes	1.76E-05	0.11	1.93E-02	5.34E+03	2.99	32.19	34.10	6%	64.26	100%
76	yes	1.76E-05	0.11	2.04E-02	5.48E+03	2.99	29.58	36.11	18%	70.49	138%
79	yes	1.76E-05	0.11	2.04E-02	1.11E+04	2.99	49.15	51.43	4%	100.39	104%
1	yes	1.75E-05	0.11	1.79E-02	2.02E+02	2.99	6.97	6.24	-12%	11.20	61%
3	yes	1.77E-05	0.10	2.20E-02	1.69E+02	2.99	6.90	6.79	-2%	13.97	102%
4	no	1.73E-05	0.12	1.48E-02	1.61E+02	2.99	6.27	4.78	-31%	7.66	22%
26	no	1.73E-05	0.12	1.46E-02	1.13E+02	2.99	3.70	3.96	6%	6.30	70%
28	no	1.77E-05	0.10	2.29E-02	2.07E+01	2.99	1.38	2.45	44%	5.18	274%
29	no	1.77E-05	0.10	2.47E-02	1.99E+01	2.99	1.54	2.56	40%	5.68	270%
27	no	1.78E-05	0.09	2.95E-02	2.03E+01	2.99	1.47	2.97	51%	7.42	406%
57	no	2.18E-05	0.07	5.19E-02	5.04E+01	2.90	16.43	7.04	-133%	24.85	51%
58	no	2.18E-05	0.11	2.19E-02	5.16E+01	2.90	7.05	3.55	-99%	6.94	-2%
59	no	2.26E-05	0.09	3.08E-02	5.39E+01	2.81	10.05	4.67	-115%	11.34	13%
40	yes	2.17E-05	0.08	3.64E-02	4.93E+02	2.94	18.91	16.68	-13%	46.18	144%
42	yes	2.22E-05	0.13	1.76E-02	5.22E+02	2.81	9.17	9.21	0%	15.54	70%
45	no	3.54E-05	0.14	8.89E-03	7.95E+02	1.79	7.46	8.18	9%	14.20	90%
46	no	3.43E-05	0.19	4.82E-03	7.83E+02	1.81	6.93	4.68	-48%	8.72	26%
55	no	3.45E-05	0.15	9.39E-03	3.22E+02	1.83	5.00	4.95	-1%	8.19	64%
53	yes	2.23E-05	0.09	3.31E-02	2.20E+02	2.85	9.18	10.06	9%	25.80	181%
54	yes	2.18E-05	0.11	2.19E-02	2.07E+02	2.90	6.14	7.12	14%	13.91	126%
61	no	2.35E-05	0.12	2.09E-02	1.08E+01	2.67	2.66	1.48	-80%	2.74	3%
60	no	2.26E-05	0.09	3.72E-02	1.06E+01	2.81	3.37	2.42	-39%	6.69	99%
63	no	3.41E-05	0.13	1.42E-02	1.46E+01	1.85	3.20	1.38	-133%	2.21	-31%
62	no	3.01E-05	0.10	3.27E-02	1.31E+01	2.08	3.33	2.16	-54%	4.95	49%
48	yes	2.16E-05	0.10	2.48E-02	8.03E+01	2.94	3.84	4.97	23%	10.60	176%
51	no	3.45E-05	0.15	9.28E-03	1.17E+02	1.83	2.71	2.95	8%	4.89	80%
36	yes	2.26E-05	0.08	4.19E-02	1.04E+02	2.81	7.30	8.32	12%	24.99	242%
50	no	3.44E-05	0.12	1.43E-02	1.28E+02	1.83	3.97	4.25	7%	6.93	75%
65	no	2.33E-05	0.10	3.11E-02	5.37E+00	2.72	2.17	1.45	-49%	3.52	62%
64	no	2.30E-05	0.07	5.48E-02	5.45E+00	2.72	3.89	2.31	-69%	8.27	113%
10	yes	1.25E-04	0.17	4.15E-02	5.50E+02	2.06	15.10	11.99	-26%	23.95	59%
72	no	3.13E-04	0.26	0.00E+00	1.81E+02	1.10	4.77	-		6.46	35%
66	no	5.99E-04	0.38	0.00E+00	8.09E+02	0.98	8.60	-		10.76	25%
67	no	4.57E-04	0.29	4.02E-02	7.54E+02	1.19	9.80	8.83	-11%	14.36	47%
68	yes	3.77E-04	0.24	5.52E-02	6.40E+02	1.40	11.59	10.72	-8%	19.94	72%
9	yes	2.95E-04	0.20	5.86E-02	6.40E+02	1.75	16.32	13.64	-20%	28.17	73%
69	no	5.66E-04	0.33	1.45E-02	4.21E+02	1.03	6.46	4.27	-51%	9.10	41%
70	no	6.03E-04	0.36	0.00E+00	5.51E+02	0.98	6.11	-		9.44	54%
71	yes	2.98E-04	0.18	6.65E-02	3.21E+02	1.75	10.02	10.84	8%	24.30	142%
8	yes	9.28E-04	0.24	1.01E-01	7.82E+02	1.42	18.61	17.46	-7%	39.91	114%
73	no	2.62E-03	0.39	0.00E+00	3.32E+02	0.84	5.98	-		11.18	87%
74	no	4.02E-03	0.54	0.00E+00	1.55E+03	0.83	9.95	-		18.21	83%
5	yes	2.24E-03	0.26	1.72E-01	8.73E+02	1.21	22.27	22.45	1%	59.93	169%
19	yes	2.20E-03	0.30	1.32E-01	4.20E+02	1.21	11.83	12.73	7%	28.54	141%
20	yes	2.22E-03	0.28	1.47E-01	2.09E+02	1.21	9.30	9.74	4%	23.42	152%
7	yes	3.71E-03	0.30	1.97E-01	8.23E+02	1.11	20.64	21.51	4%	56.09	172%
6	yes	5.41E-03	0.31	2.54E-01	8.67E+02	1.05	22.63	24.48	8%	69.53	207%
15	yes	5.21E-03	0.38	1.65E-01	3.58E+02	1.05	9.20	11.32	19%	24.17	163%
11	yes	8.84E-03	0.36	2.71E-01	7.54E+02	0.97	22.51	21.66	-4%	57.46	155%
21	yes	8.74E-03	0.38	2.41E-01	3.59E+02	0.97	12.96	13.65	5%	33.45	158%
33	yes	9.45E-03	0.41	2.30E-01	1.95E+02	0.96	8.05	9.44	15%	21.97	173%
22	yes	1.29E-02	0.36	3.73E-01	8.49E+02	0.92	24.23	27.07	10%	81.91	238%
16	yes	1.27E-02	0.39	3.13E-01	2.95E+02	0.92	13.86	14.00	1%	37.64	172%
30	yes	1.34E-02	0.31	5.55E-01	1.69E+02	0.92	21.05	16.10	-31%	63.78	203%
17	yes	1.39E-02	0.35	4.26E-01	3.51E+02	0.92	21.17	19.11	-11%	62.49	195%

4.5. Extension of correlation to the quenching sequence for case 1 tests

As already mentioned, for some ms after the peak heat flux, the wire temperature can be assumed as axially uniform, so the correlation can be used to calculate the wire cooling during this period of time.

For the so-called case 1 tests, two experimental behaviours are observed:

- a slight increase of the heat transfer coefficient during the quenching for 30 out of 47 case 1 tests (green in Table 3)
- a slight decrease of the heat transfer coefficient for 17 tests (red in Table 3). These tests are mainly at low pressure ($P < 10$ bar) and with the largest diameter ($D = 250\ \mu m$)

Our explanation is that, for these tests, the hypothesis that vaporization negligible is less correct. If some part of the heat flux lost by the wire is used for vaporization, as this part will decrease and even disappear during quenching, the heat flux decrease will

be larger in these cases which leads to a decrease of the heat transfer coefficient even if the heat transfer coefficient associated to the convection in the liquid increases as observed for 30 green tests.

Such a behaviour (slight decrease or increase of the heat transfer coefficient) is for example observed in Fig. 6 for tests T1 (1b; 96 μm; 2 m/s; 2460 K; 293 K – $q_{peak} = 24$ MW/m^2) and T3 (1b; 1.7 m/s; 2150 K; 293 K – $q_{peak} = 17.5$ MW/m^2) which have almost similar control parameters except for the wire temperature at peak heat flux. In Fig. 6, it is observed that the heat flux decrease is 2 times higher for T1 with the higher wire temperature which leads to a slight decrease of the heat transfer coefficient (the attenuation of the vaporization part being higher that the increase of the liquid heating part).

Nethertheless, in the absence of a detailed film boiling model which is the only way to evaluate the heat flux partition between vaporization and liquid heating, this new correlation can be used to get an order of magnitude of the heat flux lost by the wire in the case of large subcooling ($A \gg 1$) even for cases with decreasing heat transfer coefficient as shown in Figs. 7 and 8.

5. Quenching behaviour

If we now look at the results of Honda experiments [2] looking for the experiment with the highest boiling heat flux and the experiment with the highest wire temperature at peak heat flux, we observe (see Table 9) that even if the wire diameter is higher (q increases when diameter decreases), if the relative velocity is smaller (q increases with velocity) and the wire temperature is smaller (q increases with wire temperature), the heat fluxes measured by Honda are higher than the TREPAM ones. This leads to the conclusion that another contribution to heat transfer than stable film boiling occurs in the Honda experiment such as liquid–solid contacts as already mentioned in their paper "…the possibility of liquid–solid contact can not be discounted even in such a high superheat region". This assumption is also supported by the estimation of the vapor film thickness by $\delta_V \sim \frac{\lambda_V \Delta T_V}{q}$ which are

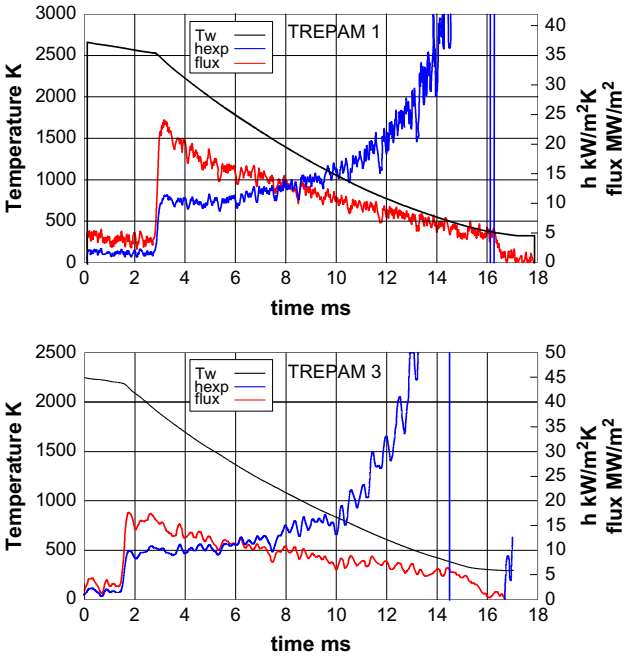

Fig. 6. Comparison of two "similar" tests except for the wire temperature at peak heat flux (T1 and T3).

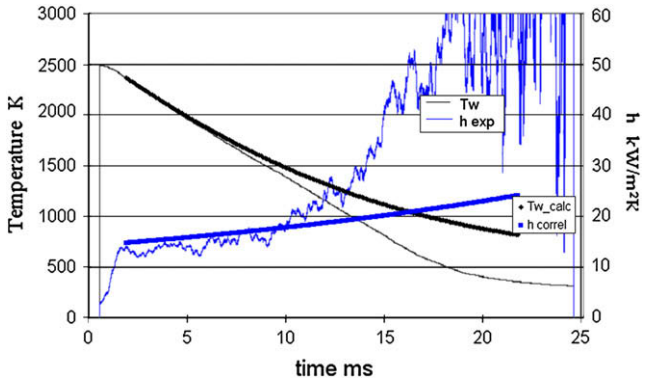

Fig. 7. Extrapolation of the correlation for the quenching sequence for a test with a slightly increasing heat transfer coefficient (T11).

~2.4 μm and 4.5 μm for the Honda test ($\frac{\delta}{D} \sim 0.01$) and 6.5 μm ($\frac{\delta}{D} \sim 0.13$) for TREPAM.

This is the reason why these tests were not included when building our correlation.

Let us now return to the results of Honda et al. who observed two types of cooling behaviour in their experiment:

- in some conditions, the heat flux increases sharply after the wire dips into the water, then it decreases gradually (see curve ABC with $T_L = 20$ °C in their Fig. 2 which is reproduced Fig. 9) up to the minimum film boiling condition.
- or, there is first a low cooling rate at high wire temperature, as for example the curve with $T_L = 50$ °C in their Fig. 2 (reproduced Fig. 9), where a low and almost constant heat flux (~2.6 MW/m^2) is observed for $\Delta T_{SAT} > 750$ °C (up to point D). Then, there is a sharp increase up to 8 MW/m^2 (D–E) before reaching a regime similar to the previous one (slow decrease of the flux) up to the classical minimum film boiling steady state condition.

From the side views of their experiment, they mentioned that the low heat flux regime at high wire temperature is associated with the presence of a vapor sheet in the wake region of the wire, vapor sheet which collapses during the cooling leading to the high heat flux regime. Differently, in the first type of cooling, the wire surface is seen to be almost completely covered with a smooth vapor film with thick and irregular vapor film and bubbles only observed near the top of the wire.

They also mentioned that the second type behaviour (two heat fluxes regime: low heat flux regime followed by a higher heat flux regime during the quenching) is favoured by low liquid velocity,

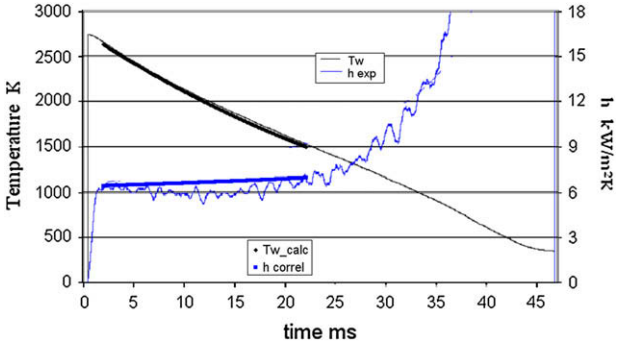

Fig. 8. Extrapolation of the correlation for the quenching sequence for a test with a slightly decreasing heat transfer coefficient (T42).

Table 9
Comparison of Honda results to a similar TREPAM test.

	P (bar)	D (μm)	U_∞ (m/s)	T_∞ (K)	q_{peak} (MW/m^2)	T_{wpeak} (K)	
Highest film boiling heat flux	1	500	1	273	20	1123	Fig. 2c of [2] curve $T_b = 0\,^\circ$C
Highest wire temperature at peak heat flux	1	500	1	293	17	1353	Fig. 7 of [2] curve $T_{WO} = 1400\,^\circ$C
Closest Trepam test (T36)	1.2	47	2	297	16.1	1520	

low wire diameter, high wire temperature and low subcooling. I would add that the two heat fluxes regime is also favoured by high pressure as, when comparing the Epstein–Hauser Nusselt numbers to TREPAM results, it is observed that $Nu_{EH} \approx 2Nu_{exp}$ when the pressure increases. That means that their non corrected results i.e. the results of their stable film boiling model, (the correlation being obtained by multiplying by 2 the model results) are in agreement with TREPAM results which are said to belong to the low heat flux region of the two region regime. It is also the case when approaching saturation as shown in their article: in the left hand part of their Fig. 2 (close to saturation), the model results get closer to the experimental results

Schematically, we can represent these two heat flux regimes as shown in Fig. 10. In some conditions (high superheat, low subcooling, low wire diameter, low velocity and high pressure), there is first a "stable" film boiling regime with vapor flow separation occurring around the wire equator so that most of heat transfer occurs on the front part of the cylinder. Then, at some time during wire cooling, something occurs that leads to an "unstable" film boiling regime surrounding all the wire which increases heat transfer. This may result from an instability growing on the vapor–liquid interface which may induce liquid–solid contacts and/or lead to the formation of droplets entrained in the rear region, both mechanisms increasing heat transfer. Development of a shear induced instability is supported by the experimental findings as large superheat and small subcooling lead to thicker thus more stable film, small velocity and high pressure (through the density ratio aspect) lead to smaller growth rate and small diameter leads to smaller growth time (the instability cannot develop sufficiently during the convection time scale)

In TREPAM, as it is not possible to follow the cooling curve for a long time due to the cooling side effects, it is likely that only the

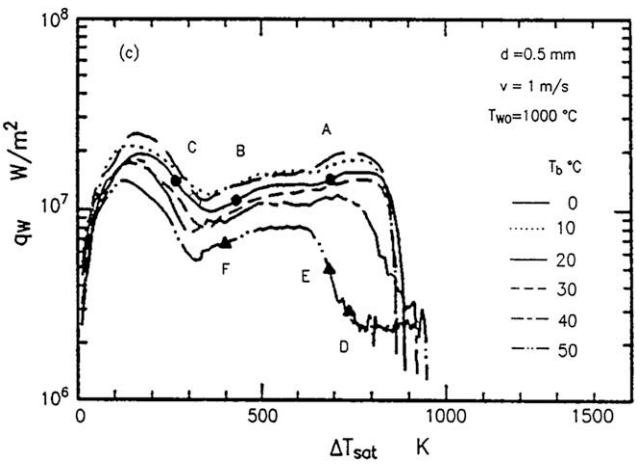

Fig. 9. Boiling curves according to coolant temperatures in Honda et al. experiment [2] (their Fig. 2).

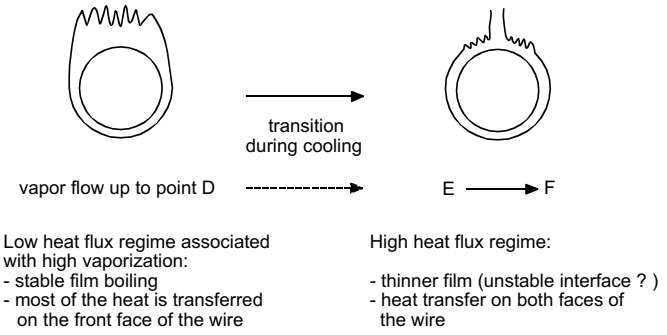

Fig. 10. Scheme of two film boiling regimes for high wire temperature quenching.

first low heat flux regime is observed (stable film boiling). This is in agreement with the fact that with a stable film boiling model [8,9], the vapor flow separates around the wire equator and also, that the above derived correlation is closer to the low heat flux domain of the Honda experiment.

It then appears that most of the film boiling experiments performed up to now may correspond to the second regime (thin – unstable? – film) which can explain the fact that the modelled stable film boiling heat fluxes have to be multiplied by 2 (Epstein–Hauser) and even more (Shigeshi et al.; Liu–Theofanous) to reproduce the measured fluxes.

This idea of a transition between very stable film boiling to a less stable film boiling allowing the possibility of transient contacts leading to an increase of heat transfer is also supported by:

- single droplet Fuel Coolant Interaction experiments devoted to the determination of the Temperature Interaction Zone i.e. the domain in the plane initial droplet temperature-initial coolant temperature leading to spontaneous vapor explosion such as the ones of Reynolds et al. [11] as shown in Fig. 11 (their Fig. 5). On this graph, the diagonal boundary is associated to the transition between a "thick film" regime and a "thin film" regime during which the coolant comes into contact with the fuel, contacts leading to the explosion.
- some film boiling experiments with hot solid tantalum and sodium by L. Caldarola in FZK [12], in which transient contacts were measured (electrically) well above the minimum film

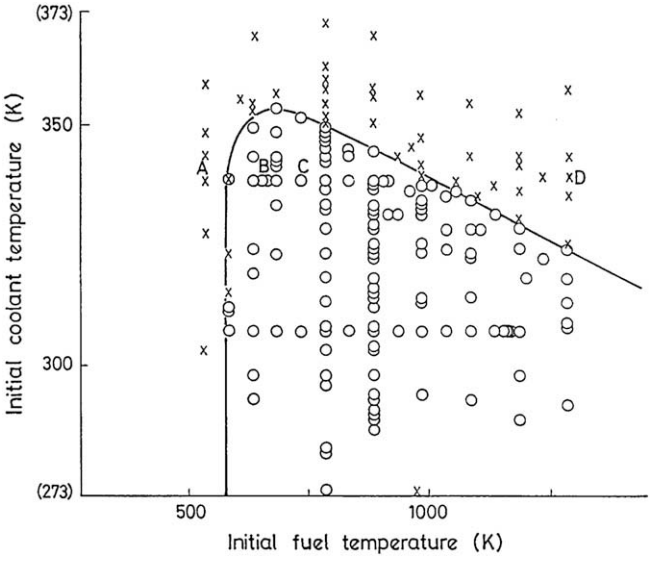

Fig. 11. Fuel-coolant interaction zone for 1.2×10^{-2} kg of tin dropped into water (0 indicates interaction, X indicates no interaction (Fig. 5 of [11])).

Table 10
Results of TREPAM supercritical tests.

Test number	P (bar)	D (μm)	U_∞(m/s)	T_W (K) peak	ΔT_V	T_∞ (K)	ΔT_∞ (K)	q_{peak} MW/m^2	Nu_{exp}	Nu_{correl}
868	240	100	1.0	2500	1845	293	361	48	14.5	13.8
884	240	250	1.1	2150	1495	293	361	27	27.8	27.1
885	240	250	1.4	2325	1670	293	361	28	24.5	28
17	210	100	1.2	1950	1307	293	350	43.3	21.2	19.1
22	200	250	1.2	2100	1461	293	346	24	24	27.1

boiling conditions, the intensity of the contacts increasing while approaching minimum film boiling. It was like if the coolant was "testing" the hot surface to know if rewetting was possible.

6. Additional tests at 240 bar

Three tests have been performed at a pressure slightly higher than the critical pressure for water (220.55 bar). Their results are presented in Table 10 and do not differ from subcritical pressure tests in quasi similar conditions (T17 at 210 bar to be compared to test 868 and T22 at 200 bar to be compared with test 884)

As these tests have been performed with cold water at 20 °C, they are considered as highly subcooled (the heat transfer coefficient increases slightly during the quenching sequence). If we define the "pseudo critical temperature" of maximum heat capacity at 240 bar i.e. 381 °C, we can separate the hot part of the coolant (called pseudo steam) from the cold part (pseudo liquid) and use the correlation established for case 1 tests with $\Delta T_V = T_w - T_{pseudocritical}$ and $\Delta T_L = T_{pseudocritical} - T_\infty$. As seen in Table 10, the agreement is pretty good.

7. Conclusions

Results of a very hot thin wire quenching experiment at varying pressures have been presented and analyzed. A simplified model of steady state stable vapor film boiling has been used to define scales to be used to correlate the results for the two extreme cases i.e. case l: most of the heat lost by the wire goes to liquid water and case 2: most of the heat is used for vaporization. As most of the tests belong to case 1, it was only possible to derive a correlation for this case of large subcooling.

It was also found that the usual film boiling correlations – based on experiments at atmospheric pressure and relatively low temperature (Tmax ~ 1000 °C) – overestimate the measured heat fluxes and an explanation is proposed to interpret the different behaviours observed during this type of quenching. In fact, in some conditions of high superheat, low subcooling, low velocity, high pressure and small wire diameter, there are two film boiling regimes. In the early times of cooling, there is a stable vapor film on the front part of the cylinder with flow separation. Then, there is a transition towards an "unstable" film surrounding all the wire with a higher heat transfer. Conditions for this transition remain to be established.

At least, results of some tests at supercritical pressure are presented.

Acknowledgements

The authors thank IRSN (Institute for Radiological Protection and Nuclear Safety) for its financial support for the TREPAM experimental program and Gilles Ratel for his help in the correlation calculations.

References

[1] G. Berthoud, Vapor explosions, Annual Review of Fluid Mechanics 32 (2000) 573–611.
[2] H. Honda, H. Takamatsu, H. Yamashiro, Heat transfer characteristics during rapid quenching of a thin wire in water, Heat Transfer Japanese Research 21 (8) (1992) 773–791.
[3] A. Inoue, Y. Fujii, S. Lee, Studies on transient film boiling heat transfer from thin wires penetrating through liquid interface, in: Proc. of International Seminar on Vapor Explosion, 1997, May 22–25, Sendai, Japan, pp. 123–130.
[4] G.K. Batchelor, An Introduction to Fluid Dynamics, Cambridge University Press, 1967.
[5] R.D. Cess, E.M. Sparrow, Film boiling in a forced convection boundary layer flow, Transactions of the ASME (August 1961) 370–376.
[6] M. Epstein, G.M. Hauser, Subcooled forced convection film boiling in the forward stagnation region of a sphere or a cylinder, International Journal of Heat and Mass Transfer 23 (1980) 179–189.
[7] T. Ito, K. Nishikawa, T. Shigeshi, Forced convection film boiling heat transfer from a horizontal cylinder to liquid cross-flowing upward (1st report: saturated liquid), Bulletin of the JSME 24 (198) (Dec 1981) 2107–2114.
[8] T. Shigeshi, T. Ito, K. Nishikawa, Forced convection film boiling heat transfer from a horizontal cylinder to liquid cross-flowing upward (2^{sd} report: subcooled liquid), Bulletin of the JSME 26 (26) (April 1983) 554–561.
[9] A. Boulin, Etude du transfert thermique lors de la trempe d'un filament à haute température à des pressions entre 1 et 210 bars, thèse Institut National Polytechnique de Grenoble, juillet 2007.
[10] C. Liu, T.G Theofanous, Film boiling on spheres in single and two phase flows, DOE/ER/12933-3 – DOE/ID – 10499, September 1996.
[11] J.A Reynolds, T.A Dullforce, R.S. Peckover, G.J. Vaughan, FCI – some basic studies at the UKAEA Culham Laboratory, CLM/RR/52/7 – SNI 6/2.
[12] L. Caldarola, private communication, 1977.